CHINESE OPTICS LETTERS

Vol. 19, No. 10 | October 2021

Broadband instantaneous multi-frequency measurement based on chirped pulse compression

Beibei Zhu (朱贝贝)[1], Min Xue (薛 敏)[1,2*], Changyuan Yu (余长源)[2], and Shilong Pan (潘时龙)[1**]

[1] Key Laboratory of Radar Imaging and Microwave Photonics, Ministry of Education, Nanjing University of Aeronautics and Astronautics, Nanjing 210016, China

[2] Department of Electronic and Information Engineering, The Hong Kong Polytechnic University, Hong Kong, China

*Corresponding author: xuemin@nuaa.edu.cn

**Corresponding author: pans@nuaa.edu.cn

Received March 15, 2021 | Accepted March 26, 2021 | Posted Online August 18, 2021

A broadband instantaneous multi-frequency measurement system based on chirped pulse compression, which potentially has a sub-megahertz (MHz) accuracy and a hundred-gigahertz (GHz) measurement range, is demonstrated. A signal-under-test (SUT) is converted into a carrier-suppressed double-sideband (CS-DSB) signal, which is then combined with an optical linearly frequency-modulated signal having the sweeping range covering the +1st-order sideband of the CS-DSB signal. With photodetection, low-pass filtering, and pulse compression, accurate frequencies of the SUT are obtained via locating the correlation peaks. In the experiment, single- and multi-frequency measurements with a measurement range from 3 to 18 GHz and a measurement accuracy of $<\pm 100$ MHz are achieved.

Keywords: instantaneous frequency measurement; chirped pulse compression; frequency-to-time mapping; microwave photonics.

DOI: 10.3788/COL202119.101202

1. Introduction

Instantaneous frequency measurement (IFM) is an essential function for emerging applications such as electronic warfare and cognitive radio systems[1]. Conventionally, IFM rapidly obtains frequency information of an unknown signal utilizing electronic techniques[2]. Restricted by narrow bandwidth and serious electromagnetic interference (EMI), the requirement of future electronic applications is hard to meet with electronics-based IFM. Photonics, featured by broad bandwidth, low loss, and EMI immunity, is a promising solution to achieve high-performance IFM[3–22]. Three different mechanisms, namely frequency-to-power mapping, frequency-to-space mapping, and frequency-to-time mapping, were proposed to realize photonics-based IFM[3–6].

Photonics-based IFM utilizing frequency-to-power mapping is a simple and widespread method[7–12]. The key point is to build a monotonic amplitude comparison function (ACF), which is used to determine the frequency of the signal-under-test (SUT) by measuring the power ratio of two optical or microwave signals. To establish a uniform frequency resolution and high-accuracy IFM system, numerous efforts were devoted to achieving an ACF with high linearity and sharp slope[8,11,12]. For instance, a high-linearity IFM with a measurement range of 3 to 18 GHz and an R-squared value as large as 0.99 was achieved by employing a silicon Fano resonator[12]. Despite all these efforts, a serious problem associated with these IFM methods is their incapability of performing multi-frequency measurement. IFM based on frequency-to-space mapping is realized by splitting the SUT into multiple space channels and then estimating its frequency[13–15]. Limited by the fineness of optical channelizers, the frequency resolution is poor. Besides, the measurement system is costly and complex due to the requirement of a photodetector (PD) array. For techniques based on frequency-to-time mapping, the IFM extracts the frequency information by detecting the electrical time delay induced by the SUT via a dispersive device[16] or a frequency shifting recirculating delay line (FS-RDL)[17,18]. The former suffers from poor resolution and low accuracy, while the latter is relatively time-consuming. To overcome the weakness of the frequency-to-time mapping method, an IFM method utilizing linear frequency modulation and pulse compression was proposed and demonstrated[19]. However, a key problem associated with this method is its incapability of multi-frequency measurement.

In this Letter, an instantaneous multi-frequency measurement method featuring broad bandwidth and high accuracy is proposed and experimentally demonstrated. Chirped pulse compression is the key to measure the frequencies precisely, which converts zero points of the waveform envelope into sharp

correlation peaks. Potentially, sub-megahertz (MHz) frequency accuracy and a hundreds-gigahertz (GHz) measurement range are achievable. In the experiments, both single- and multi-frequency measurements are performed. Frequency accuracy better than ±100 MHz within a frequency measurement range of 3 to 18 GHz is achieved. Last but not least, the importance of the length of the time window in achieving highly accurate frequency measurements needs to be pointed out. Recently, many approaches to short time window measurements of radio frequencies have been proposed, such as a compressive sensing system that achieved 100 MHz resolution in a 5 ns time window and tens of kilohertz (kHz) resolution in a microsecond time window[23], a speckle-based system that achieved similar resolution at camera frame rates[24], a spectral hole burning method with a time resolution below 100 μs[25], and a sampling and dispersive system able to intercept nanosecond-duration frequency transients in real time[26]. In our experiment, the time window is 20 μs, which is the period of the reference signal and much longer than the width of the chirped photocurrent signal. Since the theoretical frequency resolution is inversely proportional to the latter, the time window is not critical in our method.

2. Principle

Figure 1 shows the schematic diagram of the proposed instantaneous multi-frequency measurement system. In the upper path, the SUT is modulated on an optical carrier from a tunable laser source (TLS) at a Mach–Zehnder modulator (MZM). By biasing the MZM at the minimum transmission point (MITP), a carrier-suppressed double-sideband (CS-DSB) signal is generated. Mathematically, the expression can be written as

$$p(t) \propto E_0 J_{-1}(\beta)\exp[j2\pi(f_0 - f_{\mathrm{SUT}})t] + E_0 J_{+1}(\beta)\exp[j2\pi(f_0 + f_{\mathrm{SUT}})t], \quad (1)$$

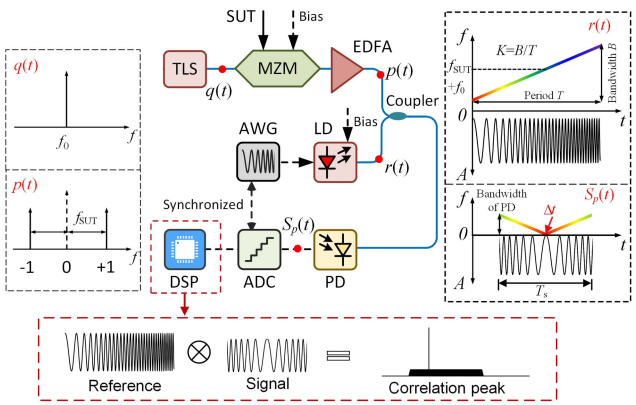

Fig. 1. Schematic diagram for the proposed instantaneous multi-frequency measurement system. TLS, tunable laser source; PC, polarization controller; SUT, signal-under-test; MZM, Mach–Zehnder modulator; EDFA, erbium-doped fiber amplifier; AWG, arbitrary waveform generator; LD, laser diode; DSP, digital signal processor; ADC, analog-to-digital converter; PD, photodetector.

where E_0 and f_0 are, respectively, the magnitude and frequency of the optical carrier. $J_{\pm1}(\bullet)$ represents the ±1st-order Bessel function of the first kind, f_{SUT} is the frequency of the SUT, and β is the modulation index.

In the lower path, a laser diode (LD) driven by a sawtooth waveform produces an optical linearly frequency-modulated (LFM) signal. Its time-domain expression is

$$r(t) = E_{\mathrm{LFM}}\exp(j2\pi f_c t + j\pi K t^2), \quad 0 \le t \le T, \quad (2)$$

where E_{LFM} is the magnitude of the optical LFM signal, T is the pulse width, and f_c and K are the center frequency and the chirp rate, respectively.

After amplification, the CS-DSB signal is coupled with the optical LFM signal. By carefully setting f_0 and f_c, the +1st-order sideband of the CS-DSB signal is located in the frequency sweeping range of the optical LFM signal while the -1st-order sideband is out of the frequency sweeping range. By square-law detection of the combined signal at a PD and extracting the low-frequency components, the frequency of the SUT is converted into a time delay carried by a low-frequency chirped signal. To simplify the processing, we let $f_0 = f_c$. In this case, the electrical field of the generated chirped photocurrent can be expressed as

$$\begin{aligned} S_p(t) &\propto \|p(t) + r(t)\|^2 \\ &\propto \mathrm{Re}\{\mathrm{rect}[(t-\Delta t)/T_s]\exp[j\pi K t^2 - j2\pi f_{\mathrm{SUT}} t]\} \\ &= \mathrm{rect}[(t-\Delta t)/T_s]\cos[\pi K(t-\Delta t)^2 - \pi K\Delta t^2] \\ &= \mathrm{Re}\{\mathrm{rect}[(t-\Delta t)/T_s]\exp[j\pi K(t-\Delta t)^2 - j\pi K\Delta t^2]\}, \end{aligned} \quad (3)$$

where $\mathrm{rect}[(t-\Delta t)/T_s]$ is a rectangular window with a width of T_s. Δt is the time delay induced by the SUT, which has a relationship with the frequency of the SUT by

$$\Delta t = f_{\mathrm{SUT}}/K. \quad (4)$$

The low-frequency chirped photocurrent is sampled by an analog-to-digital converter (ADC). Then, the chirped pulse compression is performed by correlating the low-frequency chirped photocurrent with a reference LFM signal. The frequency of the reference LFM signal should cover zero to the largest possible frequency of the chirped signal, given by

$$S_r(t) = \mathrm{Re}[\mathrm{rect}(t/T)\exp(j\pi K t^2)]. \quad (5)$$

Mathematically, the correlation function is

$$\begin{aligned} R(t) &= S_p^*(-t) \cdot S_r(t) \\ &= \frac{1}{2}\alpha(t)\mathrm{sinc}[\pi K(\Delta t + t)\alpha(t)]\cos(2\pi\gamma t + \varphi), \end{aligned} \quad (6)$$

where $\alpha(t)$, γ, and φ are given by

$$\alpha(t)=\begin{cases}(T_s+T)/2+t+\Delta t, & -(T_s+T)/2-\Delta t\le t<(T_s-T)/2-\Delta t\\ T_s, & (T_s-T)/2-\Delta t\le t<(T-T_s)/2-\Delta t\\ (T_s+T)/2-t-\Delta t, & (T-T_s)/2-\Delta t\le t<(T_s+T)/2-\Delta t\\ 0, & \text{otherwise}\end{cases},\tag{7}$$

$$\gamma=\begin{cases}K(T_s-T)/4, & -(T_s+T)/2-\Delta t\le t<(T_s-T)/2-\Delta t\\ K(t/2+\Delta t), & (T_s-T)/2-\Delta t\le t<(T-T_s)/2-\Delta t\\ K(T_s+T)/4, & (T-T_s)/2-\Delta t\le t<(T_s+T)/2-\Delta t\\ 0, & \text{otherwise}\end{cases},\tag{8}$$

and

$$\varphi=\begin{cases}\pi K\Delta t[\Delta t-(T-T_s)/2], & -(T_s+T)/2-\Delta t\le t<(T_s-T)/2-\Delta t\\ 2\pi K\Delta t^2, & (T_s-T)/2-\Delta t\le t<(T-T_s)/2-\Delta t\\ \pi K\Delta t[\Delta t+(T-T_s)/2], & (T-T_s)/2-\Delta t\le t<(T_s+T)/2-\Delta t\\ 0, & \text{otherwise}\end{cases}.\tag{9}$$

The correlation function is a Sinc function, which has the first zero points located at $t+\Delta t=\pm 1/B$, where $B=KT_s/2$ is the bandwidth of the LFM signal. Thus, the width of the compressed pulse is defined as $\tau=2\times 1/(2B)=1/B$, and the theoretical frequency resolution is $K\tau=2/T_s$. This mathematically establishes the relationship between the peak location and the delay induced by the SUT. Thus, by locating the sharp correlation peak, the time delay is obtained. Further, the frequency of the SUT is correspondingly calculated according to Eq. (4).

It is worth mentioning that, benefiting from the chirped pulse compression, the correlation peak becomes sharp, and the location accuracy is greatly improved, leading to great improvement of the frequency identify accuracy. Moreover, multi-frequency measurement is achievable, as the correlation peaks introduced by different frequencies are distinguishable.

3. Experiment

An experiment is carried out. A TLS (Anritsu MG9638A) emits a 1544.485 nm lightwave with an optical power of 8-dBm. An MZM with a 3-dB bandwidth of 20 GHz (JDS Uniphase, Model 10023874) is used to convert an SUT produced by a microwave signal generator (Agilent E8254A) into a CS-DSB signal. An optical LFM signal owning a pulse width of 20 μs (chirp rate $K=1$ GHz/μs) is generated by an optical LFM generator comprised by an electrical arbitrary waveform generator (AWG, Agilent 33250A), a homemade trans-conductance amplifier (TCA), and a commercial LD (FU-641SEA-1). A 10-GHz PD (Nortel Inc.) followed by a 1.2-GHz low-pass filter is used to achieve optical-to-electrical conversion and low-frequency component extraction. Thus, the theoretical frequency resolution is $K/B=0.83$ MHz. A real-time oscilloscope (Agilent DSO-X 93204A) is employed to record the generated photocurrent, which also functions as an ADC.

Figure 2 shows the single- and multi-frequency measurement results achieved by the proposed IFM method. When tuning the frequency of the SUT from 3 to 18 GHz with a frequency step of 1 GHz, the waveforms of the generated low-frequency photocurrents are shown in Fig. 2(a). As can be seen, the zero points of the waveform envelopes are observable, which have time delays depending on the frequencies of the SUT. For example, when a 7-GHz SUT is applied to the measurement system, the zero point can be easily recognized but difficult to precisely locate, as shown in Fig. 2(b). It is because the frequency together with the amplitude of the generated chirped photocurrent approaches zero around the zero point. To precisely identify the location of the zero point, pulse compression achieved by correlating the chirped photocurrent with the LFM signal is performed. Benefitting from the compression ratio of 2880, the zero point can be accurately localized by the correlation peak, as shown in Fig. 2(c). According to the location of the correlation peak, the frequency of the SUT is calculated to be 7.056 GHz, which is obviously more accurate than that achieved by directly observing the zero point. To demonstrate the multi-frequency measurement capability, a multi-frequency signal comprised of 13 and 18 GHz components is used to serve as the SUT. After chirped pulse compression, two correlation peaks are obtained, which can be clearly distinguished, as shown in Fig. 2(d). The measured frequencies are, respectively, 13.065 GHz and 18.033 GHz, indicating that the accuracy has no deterioration in the multi-frequency measurement. Furthermore, holding one frequency fixed at 3 GHz and sweeping a second frequency from 4 to 18 GHz in steps of 1 GHz, the

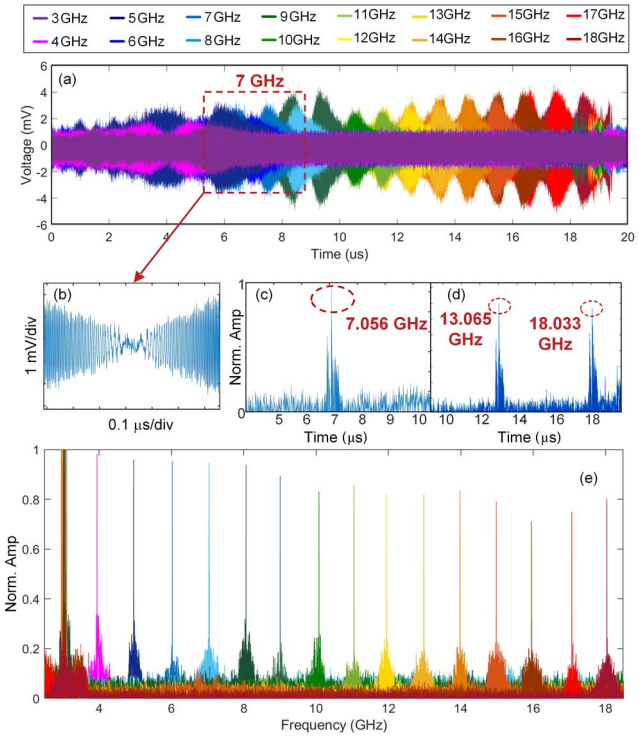

Fig. 2. (a) Waveforms of the photocurrents when tuning the frequency of the SUT from 3 to 18 GHz; (b) the zoom-in view of the zero point; (c) the correlation peak for 7 GHz SUT; (d) the two correlation peaks of a multi-frequency signal comprising 13 and 18 GHz components; (e) measurement results of a fixed 3 GHz component plus a sweeping second frequency.

measurement results are shown in Fig. 2(e), which demonstrates the capability for multi-frequency measurement over a full band (3–18 GHz).

Figure 3 shows the experimentally measured frequencies and measurement errors. As can be seen, the measured frequencies from 3 to 18 GHz are linearly fitted. The *R*-square is as large as 0.99995, which indicates that the measurement system has high linearity. Additionally, the frequency accuracy is better than ±100 MHz, as shown in Fig. 3. It should be noted that the

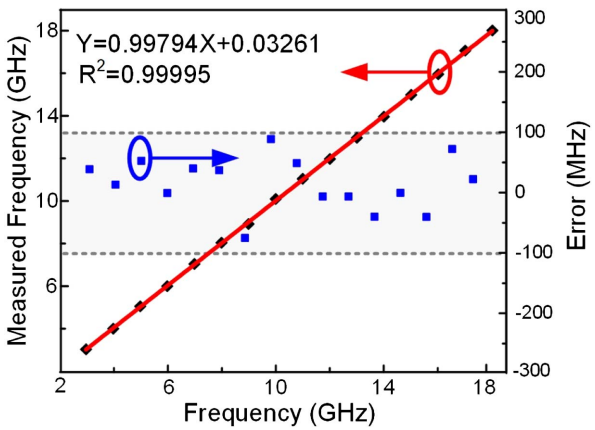

Fig. 3. Measured results with linear fitting and the measurement errors.

measurement accuracy of the proposed IFM method can be much higher. However, the relatively poor frequency stabilities of the TLS and the LD in the measurement system introduce considerable measurement errors. On the one hand, the TLS and the LD are free-running. The frequency detuning drifts the zero point and induces the major measurement error. On the other hand, the optical frequency-swept signals emitted from the LD at the same driving current in different sweeping periods have slight frequency differences, which introduce additional delay for the zero points and contribute additional measurement error. It is believed that, by employing a photonics-based LFM source[27] and synchronizing the two optical sources, the frequency accuracy can be dramatically improved by tens or even hundreds of times. Potentially, the frequency accuracy up to sub-MHz is achievable. Additionally, a hundred-GHz measurement range is available if a high-speed modulator and a broadband optical LFM source are adopted. The single measurement time is mainly determined by the pulse width of the optical LFM signal, which is 20 μs in the experiment. The measurement can be sped up if an optical LFM signal having a large chirped rate is employed.

4. Conclusion

In conclusion, an instantaneous multi-frequency measurement method based on chirped pulse compression was proposed and experimentally demonstrated. Instantaneous single- and multi-frequency measurements were successfully achieved in the experiment. The measurement results show a frequency accuracy of better than ±100 MHz within a frequency measurement range from 3 to 18 GHz. Potentially, sub-MHz accuracy and a hundred-GHz measurement range are available in theory. It is worth mentioning that, by employing optical time-division multiplexing and radio over fiber (RoF), the multi-SUT and remote measurements are achievable, which would be attractive to the distributed systems such as distributed radar systems and electronic warfare systems.

Acknowledgement

This work was supported in part by the Postgraduate Research and Practice Innovation Program of Jiangsu Province (No. KYLX16_0367), the National Natural Science Foundation of China (Nos. 62071226 and 61971372), the Hong Kong Scholar Program (No. G-YZ2S), and HK RGC GRF (No. 15200718).

References

1. D. Zhu and S. L. Pan, "Broadband cognitive radio enabled by photonics," J. Lightwave Technol. **38**, 3076 (2020).
2. P. W. East, "Fifty years of instantaneous frequency measurement," IET Radar Sonar Navigat. **6**, 112 (2012).
3. J. Yao, "Microwave photonics," J. Lightwave Technol. **27**, 314 (2009).
4. X. Zou, B. Lu, W. Pan, L. Yan, A. Stöhr, and J. Yao, "Photonics for microwave measurements," Laser Photon. Rev. **10**, 711 (2016).

5. H. Emami, M. Hajihashemi, S. E. Alavi, and M. Ghanbarisabagh, "Simultaneous echo power and Doppler frequency measurement system based on microwave photonics technology," IEEE Trans. Instrum. Meas. **66**, 508 (2017).
6. S. Pan and J. Yao, "Photonics-based broadband microwave measurement," J. Lightwave Technol. **35**, 3498 (2017).
7. X. Zou, S. Pan, and J. Yao, "Instantaneous microwave frequency measurement with improved measurement range and resolution based on simultaneous phase modulation and intensity modulation," J. Lightwave Technol. **27**, 5314 (2009).
8. Z. Li, C. Wang, M. Li, H. Chi, X. Zhang, and J. Yao, "Instantaneous microwave frequency measurement using a special fiber Bragg grating," IEEE Microwave Wireless Compon. Lett. **21**, 52 (2011).
9. D. P. Wang, K. Xu, J. Dai, Z. L. Wu, Y. F. Ji, and J. T. Lin, "Photonic-assisted approach for instantaneous microwave frequency measurement with tunable range by using Mach–Zehnder interferometers," Chin. Opt. Lett. **11**, 020604 (2013).
10. X. Y. Han, S. T. Zhang, C. Tong, N. N. Shi, Y. Y. Gu, and M. S. Zhao, "Photonic approach to microwave frequency measurement with extended range based on phase modulation," Chin. Opt. Lett. **11**, 050604 (2013).
11. B. W. Zhang, X. C. Wang, and S. L. Pan, "Photonics-based instantaneous multi-parameter measurement of a linear frequency modulation microwave signal," J. Lightwave Technol. **36**, 2589 (2018).
12. B. Zhu, W. Zhang, S. Pan, and J. Yao, "High-sensitivity instantaneous microwave frequency measurement based on a silicon photonic integrated Fano resonator," J. Lightwave Technol. **37**, 2527 (2019).
13. S. T. Winnall, A. C. Lindsay, M. W. Austin, J. Canning, and A. Mitchell, "A microwave channelizer and spectroscope based on an integrated optical Bragg-grating Fabry–Pérot and integrated hybrid Fresnel lens system," IEEE Trans. Microwave Theory Technol. **54**, 868 (2006).
14. J. M. Heaton, C. D. Watson, S. B. Jones, M. M. Bourke, C. M. Boyne, G. W. Smith, and D. R. Wight, "Sixteen channel (1- to 16-GHz) microwave spectrum analyzer device based on a phased array of GaAs/AlGaAs electro-optic waveguide delay lines," Proc. SPIE **3278**, 245 (1998).
15. X. Zou, W. Li, W. Pan, L. Yan, and J. Yao, "Photonic-assisted microwave channelizer with improved channel characteristics based on spectrum controlled stimulated Brillouin scattering," IEEE Trans. Microwave Theory Technol. **61**, 3470 (2013).
16. L. V. Nguyen, "Microwave photonic technique for frequency measurement of simultaneous signals," IEEE Photon. Technol. Lett. **21**, 642 (2009).
17. T. A. Nguyen, E. H.W. Chan, and R. A. Minasian, "Instantaneous high-resolution multiple-frequency measurement system based on frequency-to-time mapping technique," Opt. Lett. **39**, 2419 (2014).
18. T. A. Nguyen, E. H.W. Chan, and R. A. Minasian, "Photonic multiple frequency measurement using a frequency shifting recirculating delay line structure," J. Lightwave Technol. **32**, 3831 (2014).
19. B. Zhu, M. Xue, C. Yu, and S. Pan, "Broadband and high-precision instantaneous frequency measurement using linearly frequency-modulated waveform and pulse compression processing," in *Asia Communications and Photonics Conference* (2019), p .1.
20. J. Shi, F. Zhang, D. Ben, and S. Pan, "Photonic-assisted single system for microwave frequency and phase noise measurement," Chin. Opt. Lett. **18**, 092501 (2020).
21. R. Wang, S. Xu, J. Chen, and W. Zou, "Ultra-wideband signal acquisition by use of channel-interleaved photonic analog-to-digital converter under the assistance of dilated fully convolutional network," Chin. Opt. Lett. **18**, 123901 (2020).
22. Y. Zhou, F. Zhang, and S. Pan, "Instantaneous frequency analysis of broadband LFM signals by photonics-assisted equivalent frequency sampling," Chin. Opt. Lett. **19**, 013901 (2021).
23. G. A. Sefler, T. J. Shaw, and G. C. Valley, "Demonstration of speckle-based compressive sensing system for recovering RF signals," Opt. Express **26**, 21390 (2018).
24. A. C. Scofield, G. Sefler, J. Shaw, and G. Valley, "Recent results using laser speckle in multimode waveguides for random projections," Proc. SPIE **10937**, 109370B (2019).
25. P. Berger, Y. Attal, M. Schwarz, S. Molin, A. Louchet-Chauvet, T. Chanelière, J.-L. L. Gouët, D. Dolfi, and L. Morvan, "RF spectrum analyzer for pulsed signals: ultra-wide instantaneous bandwidth, high sensitivity, and high time-resolution," J. Lightwave Technol. **34**, 4658 (2016).
26. S. R. Konatham, R. Maram, L. R. Cortés, J. H. Chang, and J. Azaa, "Real-time gap-free dynamic waveform spectral analysis with nanosecond resolutions through analog signal processing," Nat. Commun. **11**, 3309 (2020).
27. S. L. Pan and Y. M. Zhang, "Microwave photonic radars," J. Lightwave Technol. **38**, 5450 (2020).